Geochemical Perspectives Letters

The stable carbon isotope fractionation of methanogenesis products at complete carbon consumption

H.K. Batther[1*], A.S. Templeton[1], T. Hoehler[2], A. Howells[2], M. Bill[3], J. Gropp[4,5], S. Kopf[1]

OPEN ACCESS

https://doi.org/10.7185/geochemlet.2543

Abstract

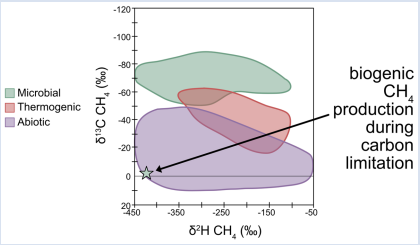

The stable carbon isotope signature ($\delta^{13}C$) of methane (CH_4) is used to discriminate between biological, thermogenic, and abiotic sources. Methanogens, or methane producing archaea, inhabit a broad range of chemical conditions. Many of these environments are replete in dissolved inorganic carbon (DIC), causing isotopically depleted $\delta^{13}C$ biogenic CH_4. However, some extreme environments inhabited by methanogens, such as serpentinising systems, exhibit low carbon dioxide (CO_2) availability, replete H_2, and isotopically enriched $\delta^{13}C$ CH_4 that is outside the known biogenic range. We measured the $\delta^{13}C$ of CO_2, biomass, lipids, and CH_4 during hydrogenotrophic methanogenesis under hydrogen replete conditions with a limited carbon pool to investigate carbon isotope dynamics at complete DIC consumption. As theory predicts, we found that the final, accumulated methane $\delta^{13}C$ values closely reflect the $\delta^{13}C$ of the initial DIC supply, and that methane is more ^{13}C enriched than biomass and lipids. This provides the first experimental evidence that methanogens can achieve complete carbon consumption and thus can produce accumulated CH_4 products that isotopically reflect the initial CO_2. These data show that the range of possible $\delta^{13}C$ values from biogenic methane needs to be expanded for natural environments impacted by extreme carbon limitation.

Received 10 June 2025 | Accepted 16 September 2025 | Published 29 October 2025

Introduction

Methane is an important energy source, greenhouse gas, and potential biosignature on Earth and other planetary bodies including Mars and Enceladus (Schulte *et al.*, 2006; Waite *et al.*, 2017). The stable isotope composition of methane is often used to distinguish between abiotic, thermogenic, and microbial sources on Earth (Schoell, 1980). However, there is ongoing debate about the isotopic range that is possible in biogenic methane (Etiope and Sherwood-Lollar, 2013), complicating interpretation of methane sources in disciplines such as natural gas exploration, origin of life studies, and extraterrestrial life detection.

Hydrogenotrophic methanogenesis, or the oxidation of H_2 to reduce CO_2 to CH_4, is the autotrophic mode of growth and most relevant methanogenesis pathway regarding the study of early Earth and the search for extraterrestrial life (Schulte *et al.*, 2006). Hydrogenotrophic methanogenesis usually results in methane with a $\delta^{13}C$ range of −110 ‰ to −60 ‰ (Elvert *et al.*, 1999; Conrad *et al.*, 2011). Factors including environmental stress, substrate availability, and metabolic reversibility control where biogenic methane plots within this range (Fuchs *et al.*, 1979; Valentine *et al.*, 2004) with metabolic net fractionation ($\varepsilon^{13}C$) estimated to range between 20 ‰ to −106 ‰ (Gropp *et al.*, 2021). In contrast, abiotic environmental methane is more ^{13}C enriched, with values as depleted as −47 ‰ to enriched positive values (Etiope and Sherwood-Lollar, 2013).

One example of environments where the source of methane remains ambiguous includes serpentinising systems, where water-rock reactions produce H_2 and CH_4 and cause extreme carbon limitation due to high alkalinity (Nothaft *et al.*, 2021). The $\delta^{13}C$ of CO_2/DIC found in natural serpentinites with high H_2 concentrations is −1.08 ‰ to −25.3 ‰ and methane detected in these systems can be relatively enriched in ^{13}C when compared to most natural environments, with $\delta^{13}C$ values as positive as +5 ‰ (Etiope and Sherwood-Lollar, 2013; Etiope *et al.*, 2016; Miller *et al.*, 2016; Nothaft *et al.*, 2021). The seemingly abiotic signal of methane in these serpentinites has sparked debate regarding the potential contribution of microbial methanogenesis since autotrophic methanogens have also been found in these systems (Miller *et al.*, 2016, 2018; Nothaft *et al.*, 2021). In theory, methanogens will produce methane with the same isotopic composition as the starting CO_2 at complete DIC consumption (Meister *et al.*, 2019). However, the lack of net carbon isotope fractionation at complete DIC consumption has not been experimentally shown. Here, we aim to address the question whether hydrogenotrophic methanogens will actually produce isotopically heavy methane in a carbon limited system.

1. Department of Geological Sciences, The University of Colorado at Boulder, CO, USA
2. Space Science and Astrobiology Division, NASA Ames Research Center, CA, USA
3. Department of Earth and Environmental Sciences, Lawrence Berkeley National Lab, CA, USA
4. Department of Molecular and Cell Biology, University of California, Berkeley, CA, USA
5. Department of Earth and Planetary Science, University of California, Berkeley, CA, USA

* Corresponding author (email: harpreet.batther@colorado.edu)

Lipids, which are utilised by all terrestrial life for energy storage and the construction of cellular membranes, are the most chemically stable polymer and can be preserved for over hundreds of millions of years within sediment (Sessions *et al.*, 2004). Like methane, lipids have carbon isotope signatures that store metabolic and/or environmental information. Carbon limitation has been seen to cause a smaller depletion in $\delta^{13}C$ of methanogen lipids when compared to carbon replete conditions, regardless of substrate (Londry *et al.*, 2008). $\delta^{13}C$ of lipids analysed from carbon limited serpentinising systems have shown ^{13}C isotopic enrichment, with an average $\delta^{13}C$ of +2 ‰ and a high of +14 ‰ compared to typically depleted values of ~−50 ‰ or less (Bradley *et al.*, 2009; Zwicker *et al.*, 2018). It is unknown whether lipids follow the same trend as methane with respect to carbon isotope fractionation under carbon limitation.

This study thus investigates the carbon isotope composition of methane, biomass, and lipids of hydrogenotrophic methanogen *Methanococcus maripaludis* S2 in a closed system under DIC limitation with excess H_2. We hypothesise that ^{13}C enriched methane should form from biological activity under extreme carbon limitation, giving rise to methane with $\delta^{13}C$ values indistinguishable from abiotic methane.

Methods

Experimental setup. Anaerobic batch cultures of *Methanococcus maripaludis* S2 were grown hydrogenotrophically in 160 mL serum vials in a modified DSMZ141 media devoid of yeast extract, cysteine, and other organic carbon sources. Cultures were given excess H_2 at 20 psi (7.4 mmol) as the electron donor and 1.08 mmol inorganic carbon ($NaHCO_3$) as the electron acceptor and sole carbon source. Cultures were continuously stirred at 625 rpm to increase the gas transfer rate between headspace and liquid. Cultures were grown at an initial pH of 6.7 and temperature of 37 °C. Optical density was measured continuously throughout growth at 630 nm. One vial was not inoculated, and the incubation was terminated immediately to capture initial DIC. Four incubations were terminated along various points of exponential growth phase. At termination, exponential cultures were injected with phosphoric acid to stop growth and release all remaining DIC into headspace. Three cultures were allowed to consume the entire DIC pool and sampled in early stationary phase. A small portion of stationary culture medium was acidified to determine if any DIC remained.

Headspace gas (CO_2, CH_4, and H_2) from acidified samples was transferred *via* gas-tight syringe to sealed serum vials filled with a 30 % NaCl solution for preservation until analysis (Gan *et al.*, 1998). After headspace sampling, biomass from stationary phase cultures was pelleted and freeze dried. Biomass pellets were divided in half for bulk biomass analysis and lipid extractions. Bulk biomass was oven dried to prepare for analysis. Lipids were extracted from biomass by acidic hydrolysis methanolysis (Zhou *et al.*, 2020). Phytane was extracted from the total lipid extract by ether cleavage and hydrogenation (Kaneko *et al.*, 2011).

Sample analyses. Headspace gases (CO_2, CH_4, and H_2) were quantified on a gas chromatograph with flame ionisation and thermal conductivity detectors (SRI GC-FID/TCD Multi-Gas #5 Configuration). $\delta^{13}C$ of CO_2 and CH_4 were measured on a Picarro Ring-Down Spectrometer G2201-I and $\delta^{2}H$ of CH_4 on a gas chromatograph isotope ratio mass spectrometry system (Thermo Scientific GC TraceGas Ultra system connected to a Thermo Scientific Delta V Plus).

Bulk biomass $\delta^{13}C$ was analysed on a Thermo Delta V continuous flow stable isotope ratio mass spectrometer attached to a Thermo Flash2000 Elemental Analyzer. Phytane was quantified on a GC flame ionisation detector (GC-FID Thermo TRACE 1310) and identified on a single quadrupole gas chromatography mass spectrometer (GC-MS Thermo ISQ LT with TRACE 1310). The $\delta^{13}C$ of phytane was measured on a GC pyrolysis isotope ratio MS (GC IsoLink II + MAT253 Plus IRMS, Thermo Scientific).

All carbon and hydrogen isotope measurements were corrected using standards of known isotopic composition and are reported in the conventional delta notation *vs.* the Vienna Pee Dee Belemnite (VPDB)/Vienna Standard Mean Ocean Water (VSMOW) international scales respectively: $\delta^{13}C = [^{13}C/^{12}C]_{sample}/[^{13}C/^{12}C]_{VPDB} - 1$; $\delta^{2}H = [^{2}H/^{1}H]_{sample}/[^{2}H/^{1}H]_{VSMOW} - 1$. Observed isotope fractionation between two reservoirs is reported in alpha and epsilon notation: $^{13}\varepsilon_{a/b} = {}^{13}\alpha_{a/b} - 1 = [^{13}C/^{12}C]_a/[^{13}C/^{12}C]_b - 1$. δ and ε values reported in per mille (‰) are implicitly multiplied by a factor of 1000 (Coplen, 2011).

Results and Discussion

During methanogenesis, CO_2 was fully consumed while H_2 remained in excess throughout the experiment. As CO_2 was consumed, the distillation process increased $\delta^{13}C$ CO_2 from −2.8 ‰ initially to +78.5 ‰ in late exponential phase (see Table 1). Conversely, methane started relatively depleted with $\delta^{13}C$ CH_4 −23.6 ‰ at the first measurement point (when ~42 % of the CO_2 was consumed) and increased to −2.5 ‰ (*i.e.* slightly above the starting value of CO_2) at the end of the distillation when the methanogens reached stationary phase and had consumed >99 % of the CO_2.

The $\delta^{13}C$ values for biomass and phytane measured in stationary phase were significantly more depleted than the methane that had accumulated at this point (Table 1), with $^{13}\varepsilon_{biomass/methane} = -5.3$ ‰ and $^{13}\varepsilon_{phytane/methane} = -16$ ‰. The biomass yield estimate from isotopic mass balance of the final

Table 1 $\delta^{13}C$ and $\delta^{2}H$ of methanogenesis products during complete carbon consumption. Stationary measurements represent 3 replicate cultures. All other measurements represent 1 culture. Errors represent the propagated standard error of the mean.

Samples	% CO_2 remaining	$\delta^{13}CO_2$ (‰)	$\delta^{13}CH_4$ (‰)	$\delta^{13}C$ (‰) phytane	$\delta^{13}C$ (‰) biomass	$\delta^{2}H$ (‰) CH_4
starting	100.0 ± 2.8	−2.8 ± 0.5				
early-exponential	57.9 ± 2.3	+15.7 ± 0.6	−23.6 ± 0.5			
early/mid-exponential	38.4 ± 2.3	+28.8 ± 0.9	−21.5 ± 0.7			
mid/late-exponential	23.6 ± 2.3	+51.2 ± 1.4	−16.1 ± 0.7			
late-exponential	13.2 ± 1.8	+78.5 ± 2.3	−12.0 ± 0.7			
stationary	0.6 ± 1.4		−2.5 ± 0.4	−18.5 ± 0.4	−7.8 ± 0.4	−437 ± 14

methane and biomass is 6.4 %, assuming no other significant sinks of carbon. This yield is lower than other estimates with abundant substrate but comparable to those with limited substrate (Londry *et al.*, 2008).

Carbon isotope fractionation between methanogenesis products. The net carbon isotope fractionation between biomass and methane measured in stationary phase is shown in Figure 1 together with literature data.

Overall, the data follows the trend that carbon limitation decreases the isotopic offset between biomass and methane. However, data from this study inverts the fractionation typically observed in laboratory experiments (Fuchs *et al.*, 1979; Summons *et al.*, 1998; Londry *et al.*, 2008; Nguyen *et al.*, 2020): methane in our cultures is more isotopically enriched than biomass (see Fig. 1; $\varepsilon < 0$ ‰/$\alpha < 1$). Fractionation between lipids and methane exhibits the same pattern (Fig. S-1).

We thus observe that extreme carbon limitation in a closed system causes the isotopic signature of accumulated biomass to be more ^{13}C depleted than methane. We hypothesise this could occur if biomass is primarily synthesised early on when there is abundant CO_2 available for both catabolism and anabolism. If methanogens prioritise the energy producing catabolic pathway of methanogenesis and reduce CO_2 fixation as CO_2 becomes limiting, the isotopic composition of biomass remains at relatively light values compared to the still accumulating methane that is produced from the increasingly enriched residual CO_2 (illustrated in Fig. 2 in the "anabolism stops" model). Although the impact of carbon limitation on biosynthesis inhibition has not been experimentally investigated in methanogens, inorganic carbon limitation has been found to increase energy producing metabolisms and decrease cell yield in ammonia oxidising bacteria to account for increased cellular maintenance energy requirements (Jiang *et al.*, 2015; Mellbye *et al.*, 2016). Additionally, hydrogenotrophic methanogens have been found to uncouple biosynthesis from methanogenesis during stressful situations, including phosphate limitation (Leigh *et al.*, 2008). As shown in Figure 2, such a decrease in biomass yield over time could cause the accumulated biomass in our experiments to be more isotopically depleted than final accumulated methane because it was predominantly produced from CO_2 early during the distillation when CO_2 was not yet as heavily ^{13}C enriched. The accumulated methane is isotopically heavier than the biomass because methane generation continued when CO_2 was sparse and ^{13}C enriched from the distillation process. This interpretation implies that the $\delta^{13}C$ of lipids and biomass may not reflect the final environmental state but rather reflect a time of high CO_2 availability.

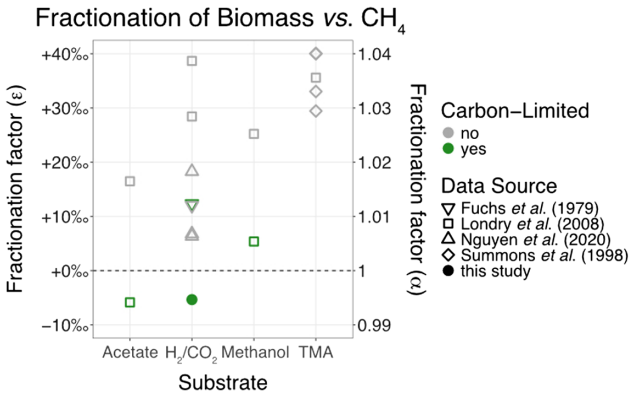

Figure 1 Carbon isotope fractionation between bulk biomass and methane from lab grown methanogens. TMA: trimethylamine.

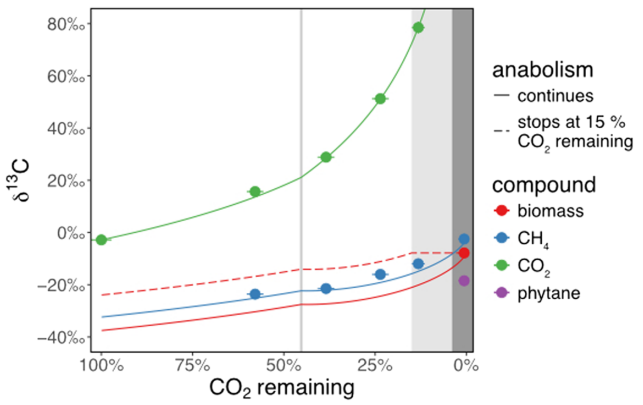

Figure 2 NLS model of CO_2 distillation during methanogenesis with $\delta^{13}C$ of substrate and accumulated products plotted against % CO_2 remaining over the course of culture growth. Lines represent modelled trends and points represent data from this study. The grey vertical line represents the step increase in metabolic fractionation that best fits the data (see text). The dark grey area represents stationary phase. The light grey area represents the stop of anabolism in the adapted model. Horizontal error bars represent standard errors. Vertical error bars are smaller than symbol sizes (Table 1).

Rayleigh distillation and CO_2 consumption. The observed isotopic compositions of methane and CO_2 fit a Rayleigh distillation model with increasing metabolic fractionation well. In its simplest form, this takes the shape of a two-step distillation process as illustrated in Figure 2 with an initial CO_2-CH_4 fractionation of -29.6 ± 2.3 ‰ that becomes more heavily fractionating (-44.0 ± 2.5 ‰) after ~55 % of CO_2 is consumed (all 3 parameters estimated simultaneously by non-linear least squares NLS data fitting in R; RMSE 2.2 ‰). This model reflects a closed system that starts with all the carbon as 100 % reactant (CO_2) and ends with 100 % products (CH_4 and biomass) and both methanogenesis and biomass production stop once all CO_2 is consumed. The total biomass yield is assumed to be the 6.4 % inferred from overall isotope mass balance. As expected from a Rayleigh distillation process, residual CO_2 and accumulated CH_4 and biomass systematically get isotopically heavier as CO_2 is consumed. The offset between the biomass and methane curves (−5.3 ‰) results from the constraint posed by the isotopic composition of the final products. At full DIC consumption, the accumulated methane is slightly enriched compared to the initial $\delta^{13}C$ of CO_2 (initial $\delta^{13}C_{CO2} = -2.8$ ‰, final $\delta^{13}C_{CH4} = -2.5$ ‰). This is the expected outcome from near complete consumption of CO_2 in a closed system for the majority product. By isotope mass balance, CH_4 will be necessarily enriched compared to CO_2 if biomass is more depleted than CO_2.

A modification of this model where anabolism stops as CO_2 becomes increasingly limiting can explain the observed isotopic composition of the accumulated biomass with a positive biomass CH_4 fractionation factor ($\varepsilon > 0$) that is consistent with literature data under non-carbon limiting conditions (Fig. 1). For example, if the methanogens stopped fixing carbon at a threshold of 15 % CO_2 remaining (example "anabolism stops" in Fig. 2), the metabolic fractionation factor between biomass CH_4 would be estimated at +8.9 ‰. The exact value of the fractionation factor depends on the threshold at which anabolism stops, which is not fully constrained by the available data (see Fig. S-2). However, based on the available literature data (Fig. 1), we hypothesise that this threshold model ("anabolism stops" in Fig. 2) is a more accurate representation of biomass

fractionation, with biomass more enriched than the accumulated methane during initial metabolism until anabolism stops and the accumulated methane continuing to get more enriched from the distillation process. The resulting estimates of the methanogenesis fractionation fall into a narrow range regardless of when anabolism stops and closely match the estimates from the simpler model ("anabolism continues" in Fig. 2): the initial fractionation is −30.0 to 29.6 ‰ and increases to −45.5 to −43.7 ‰ after ~55 % of CO_2 is consumed. These CO_2-CH_4 fractionation factors fall well within the possible range of methanogenic fractionation (−106 ‰ to −20 ‰, Gropp *et al.*, 2021). See SI for all equations and github.com/KopfLab/2025_batther_et_al._C_limitation for implementation.

Environmental implications. These experimental findings and comparison to model predictions show that biological CH_4 can span the full range of $\delta^{13}C$ CH_4 space depending on carbon availability and environmental conditions, such as hydrogen availability, rather than being constrained by the previously inferred microbial range (Fig. 3). The potential biogenicity of methane cannot be ruled out even if there is little isotopic fractionation between methane and the bulk carbon pool of any system. Rather, the lack of isotopic fractionation may be more indicative of extreme carbon limitation controlling the methane producing reaction pathway. Although such carbon limitation may be rare, environments such as serpentinising systems are an excellent example on Earth that may also be relevant to habitable rocky bodies in our solar system, and where the potential for microbial methanogenesis to produce ^{13}C enriched methane has proven to be controversial. Therefore, the $\delta^{13}C$ of CH_4 detected in the environment cannot be the sole measurement used to determine the source of CH_4, especially to rule out microbial activity. Given possible overlap with the large range of $\delta^{13}C$ CH_4 formed from Fischer-Tropsch type reactions (Etiope and Sherwood-Lollar, 2013), multiple measurements will be required to determine the biogenicity of CH_4, including analysis of the Schultz-Flory distribution of higher hydrocarbons, gene sequencing, lipidomics, or clumped CH_4 measurements (Nothaft *et al.*, 2021). However, if active biological CH_4 production can be confirmed, then the $\delta^{13}C$ of CH_4 can be used to infer if an environment is carbon limited or carbon replete.

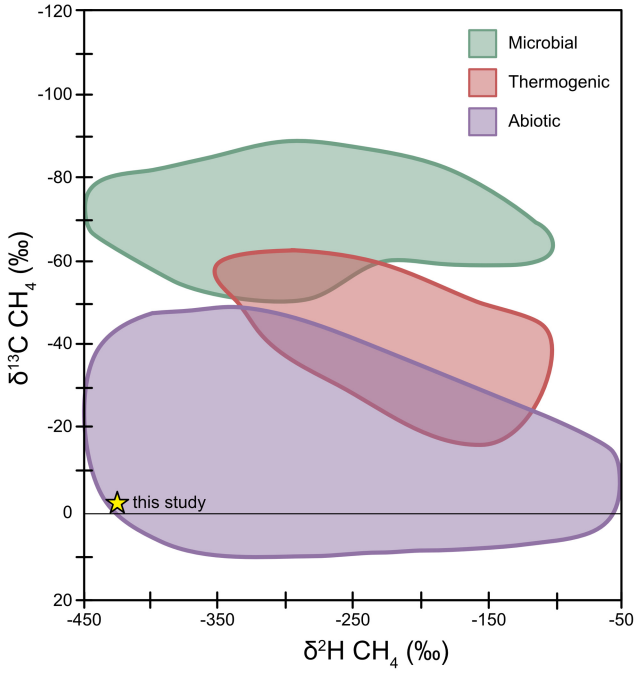

Figure 3 $\delta^{13}C$ *vs.* $\delta^{2}H$ plot of CH_4 based on Wilkes (2020) with data from Whiticar (1999); Etiope *et al.* (2016); Milkov and Etiope (2018); Miller *et al.*, (2018), and this study (yellow star).

Conclusion

This study experimentally demonstrates the impact of full carbon consumption on the carbon isotope signatures of CH_4, biomass, and lipids accumulated during purely autotrophic methanogenesis. The data show that carbon limitation causes accumulated CH_4 to isotopically reflect initial CO_2, which is supported by our Rayleigh Distillation model and has only been previously theorised. This can result in the production of biogenic methane tens of per mille more positive than traditionally assumed. Such ^{13}C enriched biogenic methane contains valuable information about the extent of C limitation, which is rarely utilised in environmental assessments. Instead, the detection of ^{13}C enriched methane has typically been attributed to abiotic sources, which may sometimes be erroneous. Additionally, we see a greater depletion of $\delta^{13}C$ biomass/lipids relative to CH_4 than expected, which could be caused by the inhibition of anabolism by carbon limitation and is an important physiological response worthy of further investigation. In summary, the data support the concept that biogenic methane, biomass, and lipid $\delta^{13}C$ values predicted for natural environments need to be significantly expanded to include the impact of extreme carbon limitation on isotope fractionation.

Acknowledgements

This work was supported by NASA Exobiology Program award #21-EXO21-0055, "Methanogenic Activity And Isotopic Biosignatures Under Carbon Limitation". The work at Lawrence Berkeley National Laboratory is supported by U.S. Department of Energy, Office of Science, Office of Basic Energy Sciences, Chemical Sciences, Geosciences, and Biosciences Division, under Award Numbers DE-AC02-05CH11231. We acknowledge the analytical contributions of the CU Boulder Earth Systems Stable Isotope Lab (CUBES-SIL) Core Facility (RRID:SCR_019300). Publication of this article was funded by the University of Colorado Boulder Libraries Open Access Fund.

Editor: Eric H. Oelkers

Additional Information

Supplementary Information accompanies this letter at https://www.geochemicalperspectivesletters.org/article2543.

Cite this letter as: Batther, H.K., Templeton, A.S., Hoehler, T., Howells, A., Bill, M., Gropp, J., Kopf, S. (2025) The stable carbon isotope fractionation of methanogenesis products at complete carbon consumption. *Geochem. Persp. Let.* 37, 35–39. https://doi.org/10.7185/geochemlet.2543

References

Bradley, A. S., Fredricks, H., Hinrichs, K., Summons, R.E. (2009) Structural Diversity of Diether Lipids in Carbonate Chimneys at the Lost City Hydrothermal Field. *Organic Geochemistry* 40, 1169–1178. https://doi.org/10.1016/j.orggeochem.2009.09.004

Conrad, R., Noll, M., Claus, P., Klose, M., Bastos, W. R., Enrich-Prast, A. (2011) Stable Carbon Isotope Discrimination and Microbiology of Methane Formation in Tropical Anoxic Lake Sediments. *Biogeosciences* 8, 795–814. https://doi.org/10.5194/bg-8-795-2011

Coplen, T.B. (2011) Guidelines and Recommended Terms for Expression of Stable-isotope-ratio and Gas-ratio Measurement Results. *Rapid Communications in Mass Spectrometry* 25, 2538–2560. https://doi.org/10.1002/rcm.5129

Elvert, M., Suess, E., Whiticar, M.J. (1999) Anaerobic Methane Oxidation Associated with Marine Gas Hydrates: Superlight C-Isotopes from Saturated and Unsaturated C 20 and C 25 Irregular Isoprenoids. *Naturwissenschaften* 86, 295–300. https://doi.org/10.1007/s001140050619

Etiope, G., Sherwood-Lollar, B. (2013) Abiotic methane on earth. *Reviews of Geophysics* 51, 276–299. https://doi.org/10.1002/rog.20011

Etiope, G., Vadillo, I., Whiticar, M.J., Marques, J.M., Carreira, P.M., Tiago, I., Benavente, J., Jiménez, P., Urresti, B. (2016) Abiotic Methane Seepage in the Ronda Peridotite Massif, Southern Spain. *Applied Geochemistry* 66, 101–113. https://doi.org/10.1016/j.apgeochem.2015.12.001

Fuchs, G., Thauer, R., Ziegler, H., Stichler, W. (1979) Carbon Isotope Fractionation by Methanobacterium Thermoautotrophicum. *Archives of Microbiology* 120, 135–139. https://doi.org/10.1007/BF00409099

Gan, J., Papiernik, S., Yates, S.R. (1998) Static Headspace and Gas Chromatographic Analysis of Fumigant Residues in Soil and Water. *Journal of Agricultural and Food Chemistry* 46, 986–990. https://doi.org/10.1021/jf970735w

Gropp, J., Iron, M.A., Halevy, I. (2021) Theoretical estimates of equilibrium carbon and hydrogen isotope effects in microbial methane production and anaerobic oxidation of methane. *Geochimica et Cosmochimica Acta* 295, 237–264. https://doi.org/10.1016/j.gca.2020.10.018

Jiang, D., Khunjar, W.O., Wett, B., Murthy, S.N., Chandran, K. (2015) Characterizing the Metabolic Trade-Off in *Nitrosomonas Europaea* in Response to Changes in Inorganic Carbon Supply. *Environmental Science & Technology* 49, 2523–2531. https://doi.org/10.1021/es5043222

Kaneko, M., Kitajima, F., Naraoka, H. (2011) Stable Hydrogen Isotope Measurement of Archaeal Ether-Bound Hydrocarbons. *Organic Geochemistry* 42, 166–172. https://doi.org/10.1016/j.orggeochem.2010.11.002

Leigh, J.A., Whitman, W.B., Hackett, M. (2008) Hydrogenases of Methanococcus Maripaludis. *U.S. Department of Energy*. https://www.hydrogen.energy.gov/docs/hydrogenprogramlibraries/pdfs/review08/besp_1_leigh.pdf?sfvrsn=77852def_1

Londry, K.L., Dawson, K.G., Grover, H.D., Summons, R.E., Bradley, A.S. (2008) Stable Carbon Isotope Fractionation between Substrates and Products of Methanosarcina Barkeri. *Organic Geochemistry* 39, 608–621. https://doi.org/10.1016/j.orggeochem.2008.03.002

Meister, P., Wiedling, J., Lott, C., Bach, W., Kuhfuß, H., Wegener, G., Böttcher, M. E., Deusner, C., Lichtschlag, A., Bernasconi, S. M., Weber, M. (2018) Anaerobic methane oxidation inducing carbonate precipitation at abiogenic methane seeps in the Tuscan archipelago (Italy). *PLoS ONE* 13, e0207305. https://doi.org/10.1371/journal.pone.0207305

Mellbye, B.L., Giguere, A., Chaplen, F., Bottomley, P.J., Sayavedra-Soto, L.A. (2016) Steady-State Growth under Inorganic Carbon Limitation Conditions Increases Energy Consumption for Maintenance and Enhances Nitrous Oxide Production in Nitrosomonas Europaea. *Applied and Environmental Microbiology* 82, 3310–3318. https://doi.org/10.1128/AEM.00294-16

Milkov, A.V., Etiope, G. (2018) Revised Genetic Diagrams for Natural Gases Based on a Global Dataset of >20,000 Samples. *Organic Geochemistry* 125, 109–120. https://doi.org/10.1016/j.orggeochem.2018.09.002

Miller, H.M., Matter, J.M., Kelemen, P., Ellison, E.T., Conrad, M.E., Fierer, N., Ruchala, T., Tominaga, M., Templeton, A.S. (2016) Modern Water/Rock Reactions in Oman Hyperalkaline Peridotite Aquifers and Implications for Microbial Habitability. *Geochimica et Cosmochimica Acta* 179, 217–241. https://doi.org/10.1016/j.gca.2016.01.033

Miller, H.M., Chaudhry, N., Conrad, M.E., Bill, M., Kopf, S.H., Templeton, A.S. (2018) Large Carbon Isotope Variability during Methanogenesis under Alkaline Conditions. *Geochimica et Cosmochimica Acta* 237, 18–31. https://doi.org/10.1016/j.gca.2018.06.007

Nothaft, D.B., Templeton, A.S., Rhim, J.H., Wang, D.T., Labidi, J., Miller, H.M., Boyd, E.S., Matter, J.M., Ono, S., Young, E.D., Kopf, S.H., Kelemen, P.B., Conrad, M.E., The Oman Drilling Project Science Team. (2021) Geochemical, Biological, and Clumped Isotopologue Evidence for Substantial Microbial Methane Production Under Carbon Limitation in Serpentinites of the Samail Ophiolite, Oman. *Journal of Geophysical Research: Biogeosciences* 126, e2020JG006025. https://doi.org/10.1029/2020JG006025

Nguyen, T.B., Topçuoğlu, B.D., Holden, J.F., LaRowe, D.E., Lang, S.Q. (2020) Lower hydrogen flux leads to larger carbon isotopic fractionation of methane and biomarkers during hydrogenotrophic methanogenesis. *Geochimica et Cosmochimica Acta* 271, 212–226. https://doi.org/10.1016/j.gca.2019.11.015

Schoell, M. (1980) The Hydrogen and Carbon Isotopic Composition of Methane from Natural Gases of Various Origins. *Geochimica et Cosmochimica Acta* 44, 649–661. https://doi.org/10.1016/0016-7037(80)90155-6

Schulte, M., Blake, D., Hoehler, T., McCollom, T. (2006) Serpentinization and Its Implications for Life on the Early Earth and Mars. *Astrobiology* 6, 364–376. https://doi.org/10.1089/ast.2006.6.364

Sessions, A.L., Sylva, S.P., Summons, R.E., Hayes, J.M. (2004) Isotopic Exchange of Carbon-Bound Hydrogen over Geologic Timescales 1 1Associate Editor: J. Horita. *Geochimica et Cosmochimica Acta* 68, 1545–1559. https://doi.org/10.1016/j.gca.2003.06.004

Summons, R.E., Franzmann, P.D., Nichols, P.D. (1998) Carbon Isotopic Fractionation Associated with Methylotrophic Methanogenesis. *Organic Geochemistry* 28, 465–475. https://doi.org/10.1016/S0146-6380(98)00011-4

Valentine, D.L., Chidthaisong, A., Rice, A., Reeburgh, W.S., Tyler, S.C. (2004) Carbon and Hydrogen Isotope Fractionation by Moderately Thermophilic Methanogens 1. *Geochimica et Cosmochimica Acta* 68, 1571–1590. https://doi.org/10.1016/j.gca.2003.10.012

Waite, H.J., Glein, C.R., Perryman, R.S., Teolis, B.D., Magee, B.A., Miller, G., Grimes, J., Perry, M.E., Miller, K.E., Bouquet, A., Lunine, J.I., Brockwell, T., Bolton, S.J. (2017) Cassini Finds Molecular Hydrogen in the Enceladus Plume: Evidence for Hydrothermal Processes. *Science* 356, 155–159. https://doi.org/10.1126/science.aai8703.

Whiticar, M.J. (1999) Carbon and Hydrogen Isotope Systematics of Bacterial Formation and Oxidation of Methane. *Chemical Geology* 161, 291–314. https://doi.org/10.1016/S0009-2541(99)00092-3

Wilkes, H. (2020) Hydrocarbons, Oils and Lipids: Diversity, Origin, Chemistry and Fate. *Cham: Springer International Publishing, Switzerland*. https://doi.org/10.1007/978-3-319-90569-3

Zhou, A., Weber, Y., Chiu, B.K., Elling F.J., Cobban, A.B., Pearson, A., Leavitt, W.D. (2020) Energy flux controls tetraether lipid cyclization in Sulfolobus acidocaldarius. *Environmental Microbiology* 22, 343–353. https://doi.org/10.1111/1462-2920.14851

Zwicker, J., Birgel, D., Bach, W., Richoz, S., Smrzka, D., Grasemann, B., Gier, S., Schleper, C., Rittmann S.K.-M.R., Kosun, E., Peckmann, J. (2018) Evidence for Archaeal Methanogenesis within Veins at the Onshore Serpentinite-Hosted Chimaera Seeps, Turkey. *Chemical Geology* 483, 567–580. https://doi.org/10.1016/j.chemgeo.2018.03.027

The Stable Carbon Isotope Fractionation of Methanogenesis Products at Complete Carbon Consumption

H.K. Batther, A.S. Templeton, T. Hoehler, A. Howells, M. Bill, J. Gropp, S. Kopf

Supplementary Information

The Supplementary Information includes:

- Methods
- Calculations
- Figures S-1 and S-2
- Supplementary Information References

Methods

Media and Culture Conditions

Methanococcus maripaludis S2 cultures were grown anaerobically and hydrogenotrophically in a modified DSMZ141 media (Deutsche Sammlung von Mikroorganismen und Zellkulturen; Braunschweig, Germany) with the following concentrations in mM: MOPS buffer, 50; $NaHCO_3$, 27; NaCl, 308; MgCl x $6H_2O$, 19.7; KH_2PO_4, 1.0287; KCl, 4.561; NH_4Cl, 4.674; $CaCl_2$ X $2H_2O$, 0.952; $Fe(NH_4)_2(SO_4)_2$, 0.005; Resazurin, 0.005; Na_2S x $9H_2O$, 2. In addition, 10 mL of DSMZ141 trace elements solution and 10 mL of DSMZ141 vitamins solution were added per litre of media. All chemicals except $NaHCO_3$, Na_2S x $9H_2O$, and DSMZ141 vitamins solution were added to the media before autoclaving. Pre-autoclave, media was stirred and boiled for 5 minutes, followed with N_2 sparging until cool to promote degassing. Then, 40 mL of media was aliquoted to N_2 sparged 160 mL serum vials containing stir bars, which were then sealed with butyl rubber stoppers and crimped shut. Post-autoclave, serum vials were sparged with H_2 for three minutes and then sterile, anoxic solutions of $NaHCO_3$, Na_2S x $9H_2O$, DSMZ141 vitamins solution were added via syringe and needle. At inoculation, 1 % culture was transferred in from a living culture with the same conditions as the experiment, and serum vial headspace was pressurized to 20 psi with H_2. In total, seven cultures were grown for this experiment, not including two negative controls.

The initial pH of the media was ~ 6.7 and cultures were kept at a temperature of 37 °C in an incubator. Serum vials were placed in Modular Internet Controllable Real-time Optical-density Loggers (microLogger) which

stirred and measured the optical density (OD) of cultures as described in Kopf and Younkin (2025). Cultures were stirred continuously at a speed of 625 rpm. OD measurements were recorded automatically every 10 min using a custom 3D-printed bottle adapter fitted with a narrow beam angle 630 nm LED (Marktech Optoelectronics, MTE7063NK2-UR) as light source and adjustable gain optical sensor (Texas Instruments, OPT101) as detector controlled by an ARM Cortex M3 powered microcontroller (Particle Industries, PHOTONH).

Of the seven cultures grown, four were terminated at various points of the growth curve and three were allowed to reach early stationary phase. Of the terminated cultures, one culture was stopped at early exponential phase, one at early-mid exponential phase, one at mid-late exponential phase, and one at late exponential phase. At termination, cultures were acidified with 0.5 mL 4 M phosphoric acid to stop growth and release all remaining DIC into the headspace. 6 mL of media from the three stationary samples was transferred to sealed, N_2 sparged 60 mL serum vials and acidified with 0.1 mL 4 M phosphoric acid to release any remaining DIC in the media into the headspace. The remaining early stationary cultures were opened and sampled immediately.

Headspace Measurements

Headspace gas from exponential cultures was sampled directly from acidified cultures and analysed immediately. Headspace gas from early stationary samples was extracted from culture vials and then transferred and stored in butyl stoppered and crimped 30 mL serum vials filled with 30 % NaCl saline solution until analysis. One negative control was acidified with 0.5 mL 4 M phosphoric to release all DIC into the headspace and analysed for initial DIC concentration measurements.

Headspace gas was run on a gas chromatograph with flame ionization and thermal conductivity detectors (SRI GC-FID/TCD 8610C Multi-Gas #5 Configuration) with argon as a carrier gas (12 psi) for quantification of CO_2, CH_4, and H_2. Pure methane gas (Airgas) and a 1 % standard gas mix of CO, CO_2, CH_4, and H_2 (Scott) were used as quantification standards. Standards were injected in multiple volumes to create calibration curves for CO_2, CH_4, and H_2. Either 25 µL or 100 µL of sample headspace was injected into the GC-FID/TCD using a N_2 sparged gas-tight syringe and needle. Samples were equilibrated with atmospheric pressure before injection. Standards and samples were run for 4 minutes at 15 °C. Each standard and sample was measured at least 3x and the final quantification value was an average of the replicate measurements.

Headspace gas was run on a Picarro Ring-Down Spectrometer G2201-I for $\delta^{13}C$ of CH_4 and CO_2. Samples were diluted with N_2 to be within the CO_2 range of 380-2000 ppm and the CH_4 range of 10-1000 ppm. Samples were diluted within a 500 mL gas-tight syringe, which was attached to the sample port so that sample could be gradually pulled into the Picarro. IAEA-C2 (- 8.24 ‰), USGS44 (- 42.21 ‰), and IAEA-603 (2.46 ‰) were used as $\delta^{13}C$ CO_2 calibration standards and three pure CH_4 gasses (- 23.6 ‰, - 38.3 ‰, and - 68.6 ‰) were used as $\delta^{13}C$ CH_4 calibration standards. Isotopic measurements of CO_2 and CH_4 on the Picarro Cavity Ringdown Spectrometer G2201-i have been factory calibrated in the presence of ambient air or ultra zero grade air, both of which have approximately 80 % N_2 and 20 % O_2. Changes in the proportion or composition of the gas matrix can rapidly change the absorbance across the spectrum. At the high sample dilution used in these measurements, the impact of H_2 and the lack of O_2 were not found to significantly impact the isotopic measurements. Each $\delta^{13}C$ value represents one measurement on the Picarro.

The hydrogen isotopic compositions (δ^2H, expressed in the VSMOW framework) of CH_4 was analysed at the Centre for Isotope Geochemistry at the Lawrence Berkeley National Laboratory using a gas-chromatograph isotope ratio mass spectrometer (GC-IRMS) system (Thermo Scientific GC TraceGas Ultra system connected

to a Thermo Scientific Delta V Plus). The methodology employed here follows that described in Turner *et al.* (2021). Briefly, headspace gas was sampled using a gas-tight syringe and injected into a 25 µL stainless-steel loop attached to a 6-port valve (VICI-Valco). The CH_4 was separated chromatographically on an HP-mole sieve fused silica capillary column (30 m ± 0.32 mm) using helium as carrier gas. Following chromatographic separation, CH_4 was passed through a ceramic tube at 1420 °C, pyrolyzed, and converted to H_2 for hydrogen isotopic measurements. Ceramic tubes were pre-conditioned by injecting 250 µL of pure CH_4 three times the day before the measurement session. Measured δ^2H values were corrected relative to external natural gas standards acquired from the United States Geological Service HCG-1 (δ^2H-CH_4 of – 64.0 ‰), HCG-2 (δ^2H-CH_4 of – 183.2 ‰), and HCG-3 (δ^2H-CH_4 of – 224.3 ‰) (Dias *et al.*, 2022).

Biomass Harvesting and Lipid Extraction

Biomass was harvested from early stationary samples through centrifugation. ~ 40 mL media was transferred to a 50 mL falcon tube and spun down at 5000 RPM for 10 minutes at 20 C, 9 ACC, and 8 DEC. After the first round of centrifugation, most of the media was discarded except 1000 µL which was used to resuspend cells. Resuspended cells were then transferred to 2 mL microcentrifuge tubes, and subsequently spun down 13,300 RPM for 10 minutes at room temperature. After the second round of centrifugation, the supernatant was discarded, and biomass pellets were frozen overnight at – 71 °C. The next day, pellets were freeze-dried for ~ 24 hours. Biomass pellets were stored at – 71 °C after being freeze-dried.

Lipids were extracted from freeze-dried biomass pellets through acidic hydrolysis-methanolysis. 1 µg of squalane was added as an internal quantification standard to biomass pellets. Pellets were physically destroyed with furnaced glass disruptor beads in a 1:1 V:V ratio with methanol for 10 minutes at 3000 RPM using a Disruptor Genie (Scientific 126 Industries, SI-DD38). Excess methanol was evaporated off before beginning acid hydrolysis. 3 M HCl with 33 % H_2O content was added to samples, which were then heated for 90 minutes at 65 °C. Methyl tert-butyl ether (MTBE) and hexane was then added to samples, followed by 5 minutes of sonification (Qsonica Q500, Newton, CT, USA). Samples were then centrifuged for 5 minutes at 15000 g at room temperature. The organic phase (hexane/MTBE) was pipetted into combusted 2 mL glass vials using a glass pipette and bulb. Hexane was added to samples two more times with centrifugation and pipetting of the organic phase. The organic phase contained total lipid extracts (TLE), which were then dried down under N_2 for ether cleavage.

For ether cleavage, hydroiodic acid was added to the dried TLE extract and heated at 120 °C for 4 hours. After heating, nanopure water and hexane were added to samples. Samples were vortexed for 1 minute and then the organic phase (hexane) was pipetted into a new set of 2 mL glass vials. The hexane addition, vortexing, and pipetting were done an additional two times. The samples were then dried down under N_2. A magnetic stir bar, PtO2, and hexane were added to each vial. Vials were bubbled with H_2 for 90 minutes. Samples were then filtered through ashed glass Pasteur pipette filter columns with glass wool and collected in 2 mL glass vials. 5 ug of quantification standard palmitic acid isobutyl ester (PAIBE) was then added to samples. Samples, which now contained the target analyte phytane, were dried under N_2 and stored at – 20 °C until isotope analysis.

Biomass and Lipid Analyses

The $\delta^{13}C$ of bulk biomass was measured on a Thermo Delta V continuous-flow stable isotope ratio mass spectrometer attached to a Thermo Flash2000 Elemental Analyzer. Oven-dried samples (~ 50 µg) and a suite of isotope standards, pugel (- 13.74 ‰), L_glut (- 26.51 ‰), EDTA2 (- 39.59 ‰), and act1 (- 29.49 ‰), were

weighed into tin capsules before being put onto the instrument. Stable isotope ratios are reported in delta (δ) notation relative to the Vienna Pee Dee Belemnite (VPDB) standard for carbon, where $\delta = ([(R_{Sample}/R_{Standard}) - 1])$, R is the ratio of the heavier mass isotope to the lighter mass isotope, as per mil (‰). In-house R scripts using R Statistical Software (v4.2.0; R Core Team 2022) and the RStudio 2022.07.0 interface (RStudio Team, 2022) with Tidyverse and IsoVerse packages (Kopf *et al.*, 2021; Wickham *et al.*, 2023) were used for data correction. Sample $\delta^{13}C$ values were corrected for either blank, offset, drift, linearity, and/or linearity+drift with a final scale correction.

Lipids were quantified on a GC-flame ionization detector (GC-FID; Thermo TRACE 1310 and identified on a GC-MS (Thermo ISQ LT with TRACE 1310). Compounds were identified on the GC-MS by comparing samples to an n-alkane mixture containing pristine and phytane. Phytane was quantified with peak size comparison between samples and quantification standards squalane and PAIBE.

The $\delta^{13}C$ of phytane was measured on a GC-pyrolysis-isotope ratio MS on a GC IsoLink 184 II IRMS System (Thermo Scientific). The GC-P-IRMS system contained a Trace 1310 GC fitted with a programmable temperature vaporization (PTV) injector, a 30 m ZB5HT column (i.d. = 0.25 mm, 0.25 µm, Phenomenex, Torrance, CA, USA), ConFlo IV interface, and MAT 253 Plus mass spectrometer (Thermo Scientific). The lipid $\delta^{13}C$ calibration was done in R, using the packages isoreader (Kopf *et al.*, 2021) and isoprocessor available at github.com/isoverse. The biomass $\delta^{13}C$ data correction and calculations were performed using in-house R scripts using R Statistical Software (v4.2.0; R Core Team 2022) and the RStudio 2022.07.0 interface (RStudio Team, 2022) with Tidyverse and IsoVerse packages (Kopf *et al.*, 2021, Wickham *et al.*, 2023).

Calculations

All calculations and data are available at https://github.com/KopfLab/2025_batther_et_al_C_limitation

Simple Rayleigh Distillation

Catabolism only

$$
\begin{aligned}
\text{Rxn: } CO_2 &\rightarrow CH_4 \\
\alpha &= \alpha_{CO2\rightarrow CH4} \\
\frac{R_{CO2}}{R_{CO2_0}} &= f^{\alpha_{CO2\rightarrow CH4}-1} \\
\text{MB: } R_{CO2_0} &= f \cdot R_{CO2} + (1-f) \cdot R_{CH4} \\
\rightarrow \frac{R_{CH4}}{R_{CO2_0}} &= \frac{1 - f \cdot R_{CO2}/R_{CO2_0}}{1-f} = \frac{1 - f^{\alpha_{CO2\rightarrow CH4}}}{1-f}
\end{aligned}
$$

Catabolism + anabolism

$$
\begin{aligned}
\text{Rxn: } CO_2 &\rightarrow (1-Y) \cdot CH_4 + Y \cdot B \\
\alpha &= (1-Y) \cdot \alpha_{CO2\rightarrow CH4} + Y \cdot \alpha_{CO2\rightarrow B} \\
&= (1-Y) \cdot \alpha_{CO2\rightarrow CH4} + Y \cdot \alpha_{B/CH4} \cdot \alpha_{CO2\rightarrow CH4} \\
&= \alpha_{CO2\rightarrow CH4} \cdot \left(1 + Y \cdot \left(\alpha_{B/CH4} - 1\right)\right) \\
&= \alpha_{CO2\rightarrow CH4} \cdot k_1 \quad | \text{ with } k_1 = 1 + Y \cdot \left(\alpha_{B/CH4} - 1\right) \\
\frac{R_{CO2}}{R_{CO2_0}} &= f^{\alpha_{CO2\rightarrow CH4} \cdot k_1 - 1} \\
R_B &= \alpha_{B/CH4} \cdot R_{CH4} \\
\text{MB: } R_{CO2_0} &= f \cdot R_{CO2} + (1-f) \cdot (1-Y) \cdot R_{CH4} + (1-f) \cdot Y \cdot R_B \\
\rightarrow \frac{R_{CH4}}{R_{CO2_0}} &= \frac{1 - f \cdot R_{CO2}/R_{CO2_0}}{(1-f) \cdot \left(1 + Y \cdot \left(\alpha_{B/CH4} - 1\right)\right)} \\
&= \frac{1 - f \cdot R_{CO2}/R_{CO2_0}}{(1-f) \cdot k_1} \\
&= \frac{1 - f^{\alpha_{CO2\rightarrow CH4} \cdot k_1}}{(1-f) \cdot k_1}
\end{aligned}
$$

Distillation with change in fractionation factors

Same as the one previous model (with anabolism and catabolism) except for the fractionation factor change at some amount of CO2 remaining f_{s1}:

$$\begin{aligned}
\text{as before: } k_1 &= 1 + Y \cdot \left(\alpha_{B/CH4} - 1\right) \\
R_B &= \alpha_{B/CH4} \cdot R_{CH4} \\
\text{new: } \frac{R_{CO2}}{R_{CO2_0}} &= \begin{cases} f^{\alpha_1 \cdot k_1 - 1} \text{ for } f \in [1, f_{a_1}] \\ f_{s1}^{\alpha_1 \cdot k_1 - 1} \cdot \left(\frac{f}{f_{s1}}\right)^{\alpha_2 \cdot k_1 - 1} \text{ for } f \in]f_{a_1}, 0] \end{cases} \\
\text{MB: } R_{CO2_0} &= f \cdot R_{CO2} + (1-f) \cdot (1-Y) \cdot R_{CH4} + (1-f) \cdot Y \cdot R_B \\
\rightarrow \frac{R_{CH4}}{R_{CO2_0}} &= \frac{1 - f \cdot R_{CO2}/R_{CO2_0}}{(1-f) \cdot k_1}
\end{aligned}$$

Adding partial anabolism

$$\begin{aligned}
\text{Step 1: } f &\in [1, f_{s1}] \\
CO_2 &\rightarrow (1 - Y_{s1}) \cdot CH_4 + Y_{s1} \cdot B \\
Y_{s1} &= \frac{Y}{1 - f_{s1}} \\
\alpha_{s1} &= (1 - Y_{s1}) \cdot \alpha_{CO2 \rightarrow CH4} + Y_{s1} \cdot \alpha_{B/CH4} \cdot \alpha_{CO2 \rightarrow CH4} \\
&= \alpha_{CO2 \rightarrow CH4} \cdot k_2 \quad | \text{ with } k_2 = 1 + Y \cdot \frac{\alpha_{B/CH4} - 1}{1 - f_{s1}} \\
\text{MB: } R_{CO2_0} &= f \cdot R_{CO2} + (1-f) \cdot (1 - Y_{s1}) \cdot R_{CH4} + (1-f) \cdot Y_{s1} \cdot R_B \\
&= f \cdot R_{CO2} + \frac{1-f}{1-f_{s1}} \cdot (1 - f_{s1} - Y) \cdot R_{CH4} + \frac{1-f}{1-f_{s1}} \cdot Y \cdot R_B \\
\rightarrow \frac{R_{CH4}}{R_{CO2_0}} &= \frac{1 - f \cdot R_{CO2}/R_{CO2_0}}{(1-f) \cdot k_2} \\
\text{still: } R_B &= \alpha_{B/CH4} \cdot R_{CH4}
\end{aligned}$$

$$\begin{aligned}
\text{Step 2: } f &\in]f_{s1}, 0] \\
CO_2 &\rightarrow CH_4 \\
\alpha_{s2} &= \alpha_{CO2 \rightarrow CH4} \\
\text{MB: } R_{CO2_0} &= f \cdot R_{CO2} + \left(f_{s1} - f + (1 - f_{s1}) \cdot (1 - Y_{s1})\right) \cdot R_{CH4} + (1 - f_{s1}) \cdot Y_{s1} \cdot R_B \\
&= f \cdot R_{CO2} + (1 - f - Y) \cdot R_{CH4} + Y \cdot R_B \\
&= f \cdot R_{CO2} + (1 - f - Y) \cdot R_{CH4} + Y \cdot \alpha_{B/CH4} \cdot R_{CH4_{s1}} \\
\rightarrow \frac{R_{CH4}}{R_{CO2_0}} &= \frac{1 - f \cdot R_{CO2}/R_{CO2_0} - Y \cdot \alpha_{B/CH4} \cdot R_{CH4_{s1}}/R_{CO2_0}}{1 - f - Y} \\
\text{new: } R_B &= \alpha_{B/CH4} \cdot R_{CH4_{s1}}
\end{aligned}$$

The overall B/CH4 fractionation factor and f_{s1} are dependent on each other by the following equation whose solution can be found numerically by root finding:

$$\frac{R_{B_{final}}}{R_{CO2_0}} = \alpha_{B/CH4} \cdot \frac{R_{CH4_{s1}}}{R_{CO2_0}} = \alpha_{B/CH4} \cdot \frac{1 - f_{s1} \cdot R_{CO2_{s1}}/R_{CO2_0}}{(1 - f_{s1}) \cdot k_2}$$

Supplementary Figures

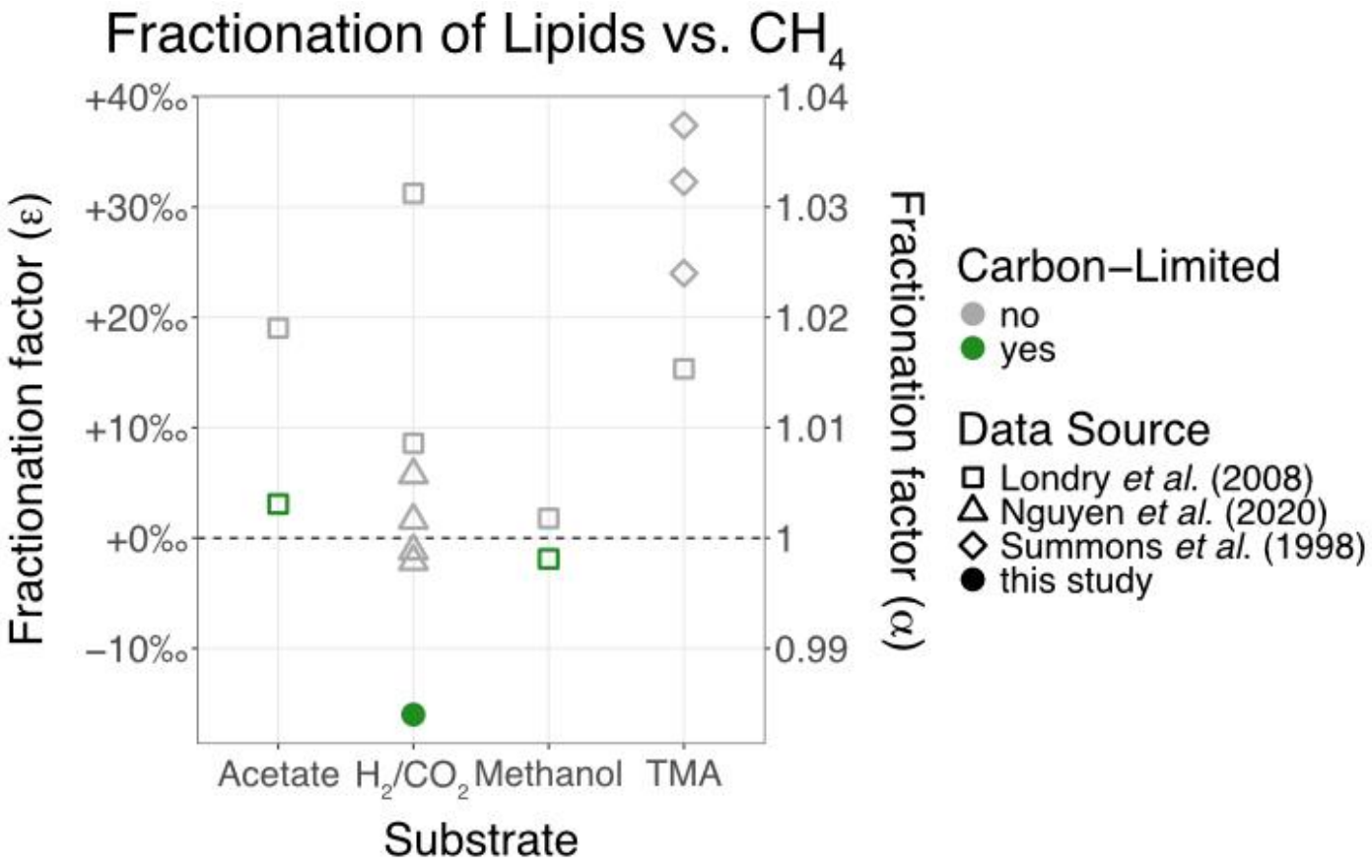

Figure S-1 Fractionation between methane and lipids from lab grown methanogen cultures from this experiment and literature data. TMA: trimethylamine.

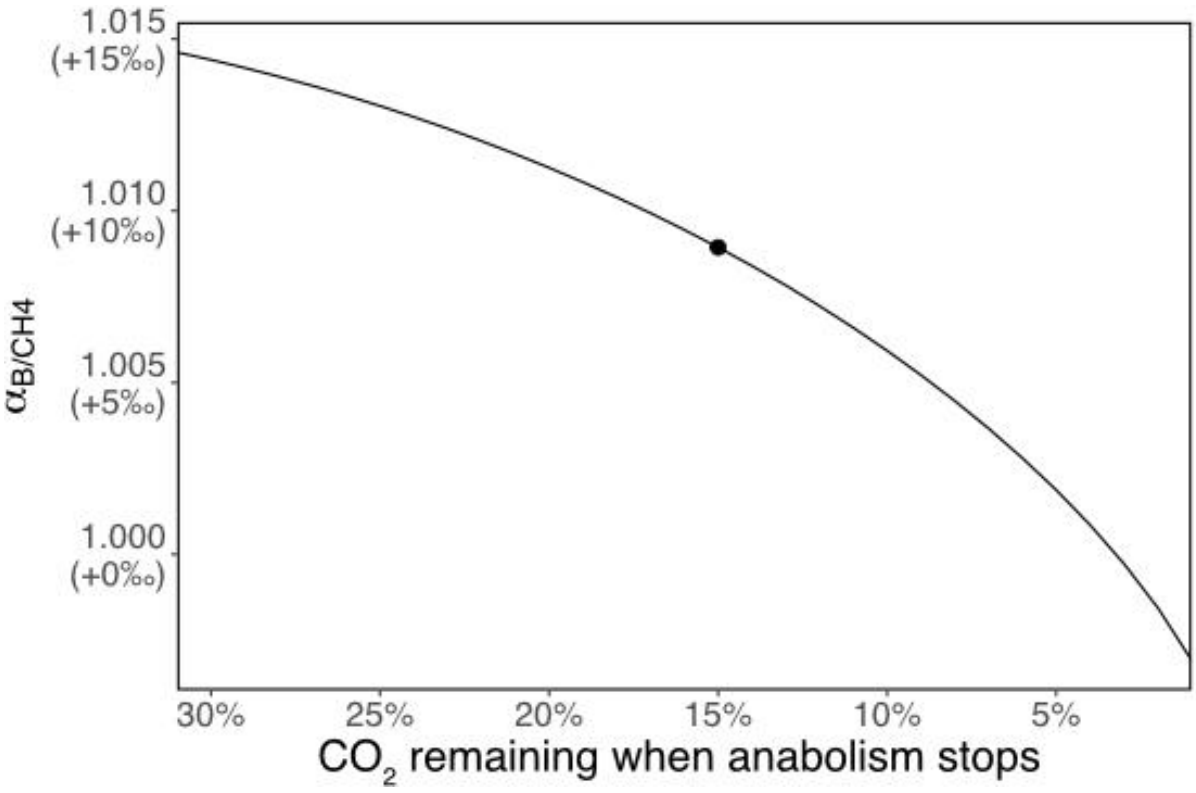

Figure S-2 Fractionation factors between biomass and methane (α) at various points of anabolism inhibition plotted against CO_2 remaining (%).

Supplementary Information References

Dias, R.F., Coleman, D.D., Ellis, G.S. (2022) Stable Isotopic Data (Delta13C and Delta2H) for Reference Materials HCG-1, HCG-2, HCG-3. *USGS Asset Identifier Service (AIS)* https://doi.org/10.5066/P9RBXUMD

Kopf, S., Younkin, A. (2025) µLogger: a Modular Internet Controllable Real-time Optical-density Logger. https://github.com/KopfLab/micrologger_device.

Kopf, S., Davidheiser-Kroll, B., Kocken, I. (2021) Isoreader: An R package to read stable isotope data files for reproducible research. *JOSS* 6, 2878. https://doi.org/10.21105/joss.02878

Londry, K.L., Dawson, K.G., Grover, H.D., Summons, R.E., Bradley, A.S. (2008) Stable Carbon Isotope Fractionation between Substrates and Products of Methanosarcina Barkeri. *Organic Geochemistry* 39, 608–621. https://doi.org/10.1016/j.orggeochem.2008.03.002

Nguyen, T.B., Topçuoğlu, B.D., Holden, J.F., LaRowe, D.E., Lang, S.Q. (2020) Lower hydrogen flux leads to larger carbon isotopic fractionation of methane and biomarkers during hydrogenotrophic methanogenesis. *Geochimica et Cosmochimica Acta* 271, 212–226. https://doi.org/10.1016/j.gca.2019.11.015

R Core Team (2022) R: A Language and Environment for Statistical Computing. *R Foundation for Statistical Computing, Vienna*. https://www.R-project.org

RStudio Team (2022) RStudio: Integrated Development for R. RStudio. *PBC*. http://www.rstudio.com/

Summons, R.E., Franzmann, P.D., Nichols, P.D. (1998) Carbon Isotopic Fractionation Associated with Methylotrophic Methanogenesis. *Organic Geochemistry* 28, 465–475. https://doi.org/10.1016/S0146-6380(98)00011-4

Turner, A.C., Korol, R., Eldridge, D.L., Bill, M., Conrad, M.E., Miller III, T.F., Stolper, D.A. (2021) Experimental and theoretical determinations of hydrogen isotopic equilibrium in the system CH_4-H_2-H_2O from 3 to 200 °C. *Geochimica et Cosmochimica Acta* 314, 223–269. https://doi.org/10.1016/j.gca.2021.04.026

Wickham, H. (2023) *Tidyverse: Easily Install and Load the Tidyverse*. https://CRAN.Rproject.org/package=tidyverse